plants

MDPI

Article

Oxygen Dynamics in the Rhizosphere of *Vallisneria spiralis* Characterized by a Fluorescent Planar Optode

Jingwei Tan [1,2,3], Zhihao Wu [1,2,3], Xiaosong Yang [1,2,3], Weidong Jin [1,2,3,*], Yiming Zhao [1,2,3] and Qing Cai [1,2,3]

[1] National Engineering Laboratory for Lake Pollution Control and Ecological Restoration, Institute of Lake Environment, Chinese Research Academy of Environmental Sciences (CRAES), Beijing 100012, China; wu_zhihao1@163.com (Z.W.)
[2] State Environmental Protection Key Laboratory for Lake Pollution Control, Institute of Lake Environment, Chinese Research Academy of Environmental Sciences (CRAES), Beijing 100012, China
[3] State Key Laboratory of Environmental Criteria and Risk Assessment, Chinese Research Academy of Environmental Sciences (CRAES), Beijing 100012, China
* Correspondence: kindong.04@163.com

Abstract

Oxygen (O_2) leakage in macrophyte rhizospheres is an adaptive strategy for hypoxic environments, which is important in lake ecological restoration. In this investigation, the fluorescent planar optode (PO) technique is used for two-dimensional (2D) distribution of dissolved O_2 at a submillimeter scale in the rhizosphere of *Vallisneria spiralis* under various environmental conditions. The spatial heterogeneity in the distribution of oxic microniches is frequently verified in the rhizosphere. The radial oxygen loss (ROL) rate for root systems is characterized by the following sequence: basal root (20.6 ± 5.1–49.6 ± 9.5 nmol m^{-2} s^{-1}, n = 7) > lateral root (14.1 ± 4.1–36.6 ± 8.3 nmol m^{-2} s^{-1}, n = 7) > root tip (13.1 ± 4.6–28.8 ± 6.4 nmol m^{-2} s^{-1}, n = 7). The O_2 maximum value on lines transecting each kind of root also obeys the sequence mentioned above. For one typical root, (1) O_2 decreases from 131.2 ± 2.4–147.4 ± 3.7 μmol L^{-1} at the root center to 47.2 ± 1.4–75.9 ± 2.2 μmol L^{-1} in the rhizosphere fringe due to O_2 supply from the root surface and O_2 consumption in rhizosphere sediment, and (2) the furthest distance from the aboveground part to the root tip leads to the lowest O_2 concentration at the root apex of that root. The light/dark transition and O_2 level in overlying water modulate the photosynthetic activity of leaves and the transfer of oxygen in the water column through aerenchyma tissue to the roots. The sequence of the oxygenated area (%), ROL rate, and O_2 concentration in rhizosphere sediment under various conditions is demonstrated as: high illumination/high O_2 > darkness/high O_2 > high illumination/low O_2 > darkness/low O_2. The effect of O_2 in water on the ROL of *Vallisneria spiralis* is more distinct than illumination. Oxygen storage in roots, and especially O_2 diffusion from overlying water, can supplement O_2 deficiency in the rhizosphere during the cessation of photosynthesis under darkness. This research advances the understanding of complex interrelationships among O_2 dynamics in different root parts, photosynthesis, O_2 in overlying water and O_2 transfer through plant aerenchyma to the rhizosphere.

Keywords: rhizosphere; *Vallisneria spiralis*; planar optode; two-dimensional; radial oxygen loss; photosynthesis

Check for updates

Academic Editor: Viktor Oláh

Received: 25 April 2026
Revised: 3 June 2026
Accepted: 11 June 2026
Published: 23 June 2026

Copyright: © 2026 by the authors. Licensee MDPI, Basel, Switzerland. This article is an open access article distributed under the terms and conditions of the Creative Commons Attribution (CC BY) license.

1. Introduction

Oxygen (O_2) can be transported to the rhizosphere of aquatic macrophytes or terrestrial plants through aerenchyma tissue [1–4]. Radial oxygen loss (ROL) in the macrophyte rhizosphere is mainly controlled by photosynthesis and O_2 consumption through the root system [5]. Photosynthetic O_2 production under light exposure controls partial O_2 pressure in the internal gas channel of the plant, leading to root O_2 leakage [6]. O_2 in overlying water maintains aerobic conditions around the roots through O_2 diffusion from overlying water when there is no O_2 supply through leaf photosynthesis during the night [7]. O_2 release in the rhizosphere can engender the formation of a spatiotemporal microoxic zone and iron (Fe) plaque on the root surface [4]. ROL can affect biogeochemical reactions in rhizosphere sediment, such as nitrification, metal mobilization, and contaminant degradation. O_2 secretion in the rhizosphere can also protect roots from the penetration of toxins [8–10].

O_2 leakage patterns in root systems are substantially different among plant species. Some aquatic plants (*Zostera marina*, *Halophila ovalis* and *Phragmites australis*) mainly secrete O_2 through the root tip [11–13]. Meanwhile, O_2 can be released from all root parts (basal root, lateral root and root tips) of *Potamogeton crispus*, *Cymodocea rotundata*, *Myriophyllum spicatum*, *Potamogeton perfoliatus* and *Vallisneria spiralis* (*V. spiralis*) [5,14–17]. O_2 depletion from the root center to the rhizosphere edge in the cross-section of a typical plant root is due to O_2 leakage from the root surface and O_2 consumption in the rhizosphere and bulk sediments [18].

Conventional techniques for the measurement of O_2 concentration in the macrophyte rhizosphere mainly include the use of needle-type microelectrodes [19,20], optical fibers [21], and the colorimetrical method [22]. However, these techniques have some inherent drawbacks, including low accuracy, complex operation, the large sample volume required, electrode brittleness, extensive replication to cover large areas, and incompatibility with two-dimensional (2D) analysis. Thus, an in situ and non-destructive technique—the planar optode (PO)—has been developed for the 2D distribution of O_2 in the rhizosphere of aquatic macrophytes. The PO system for O_2 measurement consists of an O_2-sensing film (luminophore immobilized in one analyte-permeable matrix coated onto a supporting material), an excitation unit, and an imaging system (camera) [23–26]. PO measurement is based on dynamic quenching of photoluminescence by O_2 under light excitation without O_2 consumption [22,27–29]. The advantages of PO measurement include cheapness, high spatial coverage (mm^2–cm^2), high spatial resolution (-μm), measurement period flexibility (seconds–days), and high selectivity and sensitivity [30].

The PO technique has been used to determine the O_2 dynamics of biological samples [31], coral [32], sediment [33], biofilms [30], animal burrows [34] and plant–root systems [12,35,36]. The measurement of the 2D distribution of O_2 in the plant rhizosphere using POs has become a research hotspot in recent years [12,35,36], and these plants include (1) aquatic macrophytes such as *Phragmites australis*, *V. spiralis* or *Potamogeton crispus* and (2) terrestrial plants such as rice plant and *Elymus athericus* [4,6,13,15,37–39]. The root-triggered redox condition influences speciation and biogeochemical reactions of nitrogen, phosphorus or trace metals in rhizosphere sediment [38,40,41].

V. spiralis is usually used for lake ecological restoration due to its high capability of O_2 leakage from roots, tolerance of trace metals and nutrients and bioaccumulation [36]. Understanding ROL patterns in various root parts of *V. spiralis* under different environmental conditions is important for elucidating its resilience and adaptability to a fluctuating environment and phytoremediation mechanisms for lake ecology.

Until now, only a few papers have reported O_2 dynamics in the rhizosphere of *V. spiralis* using the PO technique [6,10,36], and the characteristics of O_2 distribution in the root zone and the driving mechanisms for ROL have not been revealed clearly.

Two questions are proposed, including: (1) Do ROL parameters and O_2 concentrations vary among different locations in the rhizosphere (basal root, lateral root, root tip or some lines across or along one typical root)? (2) What are the influences of the light/dark transition and O_2 levels in overlying water on ROL in various root parts and the driving mechanisms? In order to answer those questions, the PO technique is used for the high-resolution quantitative characterization of the 2D O_2 distribution in the rhizosphere of *V. spiralis* in this investigation. The research results should improve our understanding of O_2 cycling at the root–sediment interface related to lake ecological remediation using aquatic macrophytes.

2. Materials and Methods

2.1. Sediment Sampling and Plant Pre-Incubation

In April 2023, sediment (thickness: 10 cm; weight: 20 kg) and overlying water (50 L) were collected using an Ekman grab sampler and an acid-cleaned polyethylene bottle, respectively, from one site in the Qing River in Beijing (China) (Figure S1, Supplementary Materials). The macrofauna and debris were removed from the sediment. The sediment was air-dried and ground to pass through a screen with a 100 μm mesh size. The sediment was mixed and homogenized. The total phosphorus (TP), total nitrogen (TN) and total iron (TFe) in the sediment were 984, 2889 and 15,854 mg kg^{-1} (dry weight), respectively. Seedlings of *V. spiralis* were purchased from Runxi Agricultural Science and Technology Co., Ltd. (Xiong'an New Area, Henbei Province, China). First, 200 mL of water and the dry sediment (0.8 kg) were mixed and put into a rhizobox (Figure 1A). The *V. spiralis* seedlings (length: 10 ± 0.4 cm; weight: 3.2 ± 0.2 g) were planted into the sediment in the rhizobox. The rhizobox was put into one experimental flume (Figure 1A) for 12 d of cultivation before PO measurement. The rhizobox was placed at an angle of 30° in the experimental flume to ensure root development along the front window of the rhizobox (Figure 1A). *V. spiralis* was cultivated at 20 °C under artificial irradiance with wave length range (350–1100 nm) by a light-emitting diode (LED) (Figure 1A) with a daily cycle of 12 h light (irradiation intensity: 150 μmol photons m^{-2} s^{-1})/12 h dark (irradiation intensity: 0 μmol photons m^{-2} s^{-1}) and O_2 (175 μmol L^{-1}) in water in the experimental flume. The irradiation intensity was measured using a light quantum meter (3415 FSE, Spectrum Technologies, Inc., Aurora, IL, USA). The detailed plant cultivation is described in the Supplementary Materials (SM A).

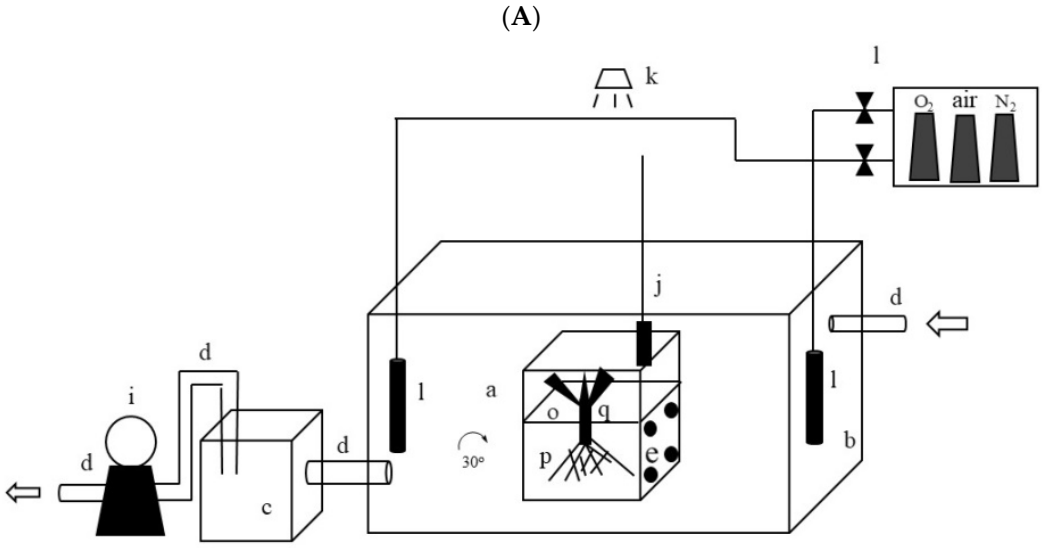


Figure 1. *Cont.*

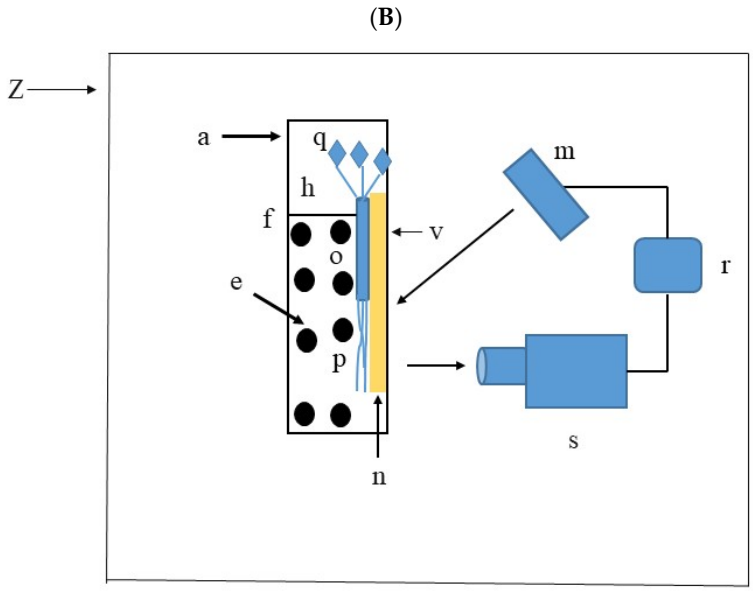


Figure 1. Schematic graphs of the experimental design. (**A**): The overall schematic graph for the experiment. (**B**): The schematic graph of the rhizobox and the planar optode (PO) instrument. (a) Rhizobox; (b) experimental flume; (c) water return tank; (d) return pipe; (e) sediment; (f) sediment/water interface; (h) water; (i) peristaltic pump; (j) O_2/T/pH electrode; (k) illumination lamp; (l) aeration device; (m) light-emitting diode (LED); (n) O_2-sensing film; (o) aquatic macrophyte; (p) root; (q) leaf; (v) detachable front window; (r) trigger box; (s) camera; (z) enclosed PO device.

2.2. Experimental Setup

After 12 d of cultivation, the rhizobox was taken out from the experimental flume, and the detachable front window was removed from the rhizobox (Figure 1). The other detachable front window with a square O_2-sensing film (8 cm × 8 cm, EasySensor) adhered to it (Figure 1) was immediately fixed in the rhizobox. Black plastic sheeting was used to cover the outside of the rhizobox to keep the rhizosphere dark. The rhizobox was put back in water in the experimental flume and maintained for 4 h under one environmental condition. Four environmental conditions were regulated by aeration equipment and an illumination lamp (Figure 1A), including illumination (200 μmol photons m^{-2} s^{-1})/O_2 (141 μmol L^{-1}), darkness (0 μmol photons m^{-2} s^{-1})/O_2 (141 μmol L^{-1}), illumination (200 μmol photons m^{-2} s^{-1})/O_2 (280 μmol L^{-1}) and darkness (0 μmol photons m^{-2} s^{-1})/O_2 (280 μmol L^{-1}). These conditions are designated as high illumination/low O_2, darkness/low O_2, high illumination/high O_2 and darkness/high O_2. A multi-parameter water quality analyzer (HQ 4300, Hach Company, Loveland, CO, USA) (Figure 1) was used to measure O_2, temperature and pH in the water in the rhizobox. The temperature and pH were 20 °C and 8.0, respectively. The irradiation intensity was measured using a light quantum meter (3415 FSE, Spectrum Technologies, Inc., Aurora, IL, USA). This light quantum meter specifically provides accurate illumination readings of PAR (photosynthetically active radiation) with a wavelength range (400–700 nm) (Figure 1).

After 4 h of cultivation, the rhizobox was retrieved from water, and the outside black plastic sheeting was removed. It was transferred to the enclosed PO device (Figure 1B) for O_2 measurement. Then, the rhizobox was put back into the experimental flume for the next 4 h of cultivation. The disturbance of O_2 in the rhizosphere sediment caused by changing the detachable front window in the rhizobox or measuring rhizosphere O_2 in the PO device mentioned above can be ignored after 1 h of cultivation in water. After PO measurement for O_2 in rhizosphere sediment under all four environmental conditions, the detachable front window of the rhizobox was removed, and a digital camera (Canon EOS 600D, Canon Inc., Tokyo, Japan) was used to take photos of the rhizosphere. The diameters

of the basal root, lateral root and root tip were measured using a digital vernier caliper (543-781, Mitutoyo Company, Takatsu-ku, Kawasaki, Kanagawa, Japan). The cultivation of *V. spiralis* and the procedures for roots and sediment after PO measurement are described in SM A (Supplementary Materials).

2.3. PO Imaging

PO measurement of oxygen is based on the dynamic quenching of a fluorophore in the presence of O_2. The O_2-sensing film with a thickness of 10 µm was made by EasySensor Ltd. (Nanjing, China) based on the method recommended in references [22,36,42,43]. First, a sensor "cocktail" is prepared by dissolving an oxygen-quenchable luminophore, i.e., a reference fluorophore coumarin C545 (C545T), Platinum (II)5,10,15,20-tetrakis-(2,3,4,5,6-pentafluorphenyl) porphyrin (PtTFPP) and polystyrene in toluene. This "cocktail" is gently stirred and then sprayed on a transparent dust-free polyethylene terephthalate using ultrasonic spray equipment [22,36]. Second, one thin layer of silicone rubber (Dow Corning 3140, Dow Corning Corporation, Midland, MI, USA) is coated on top of this dry sensing membrane as a protective layer [36]. Detailed information on the O_2-sensing film mentioned above can be found in SM B.

The PO device (Easysensor PO 2100) (Figure 1B) was purchased from EasySensor Ltd. (Nanjing, China). The PO device contains a Complementary Metal Oxide Semiconductor (CMOS) camera with a 460 nm long-pass filter, two light-emitting diodes (LEDs) (390–400 nm), a PC-controlled trigger box for the camera and LEDs, and a darkroom. The recorded fluorescence image with a 2D spatial resolution of 62 × 62 µm is calibrated using the fluorescence intensities of the known O_2 concentrations (0% and 100% O_2 saturation in water) at 20 °C, using a modified Stern–Volmer equation (Equation (1)) [44].

$$\frac{R}{R_0} = \alpha + (1-\alpha)\frac{1}{1+K_{SV}C} \quad (1)$$

where R and R_0 are the fluorescence intensity ratio (red/green) at an O_2 concentration of C (%, air saturation) and C_0 (0%, air saturation), respectively. C is the O_2 concentration, K_{sv} is the Stern–Volmer quenching constant, and α is the non-quenchable fraction of the fluorescence signal, which is temperature independent. Details of the calibration and calculation of the O_2 optode are provided in SM B.

2.4. Data Analysis

The fluorescent image was processed using Image J. 1.53 (http://rsb.info.nih.gov/ij/, accessed on 2 March 2023) and divided into red, green and blue channels. The red/green ratio at each point in the fluorescent image was converted to O_2 concentration by calibration (SM B). The detection limit of PO analysis (2.20 µmol L^{-1}) is quantified as three times the standard deviation (3SD) of the measured concentration in an anoxic area of the fluorescent image (about 1% air saturation; n = 7). The point where the O_2 concentration drops below 2.20 µmol L^{-1} is considered to be the O_2 penetration depth (OPD) (mm) across the sediment/water interface (SWI) and the root/sediment interface. The diffusive O_2 uptake (DOU) (nmol m^{-2} s^{-1}) is derived according to the vertical O_2 concentration profile at the SWI and Fick's first law of diffusion (Equation (2)) [13]:

$$\mathrm{DOU} = \phi \times \mathrm{Ds} \times \frac{\partial C}{\partial z} \quad (2)$$

where ϕ represents the sediment porosity derived using the method (SM A) proposed in reference [45]; ϕ equals 0.81 ± 0.03 (n = 7) for the rhizosphere sediment in this experiment;

Ds (cm^2/s) is the molecular diffusive coefficient of O_2 in sediment, and it can be calculated by Equation (3) [46]:

$$D_s = \phi^2 D_0 \quad (3)$$

D_0 is the oxygen diffusive coefficient in water, and $\partial C/\partial z$ is the O_2 concentration gradient. In this investigation, seven O_2 vertical profiles in each 2D image of the O_2 distribution (for example, Figure S2) were chosen for derivation of $\frac{\partial C}{\partial Z}$. The average volume-specific O_2 consumption (R_{SWI}) (μmol m^{-3} s^{-1}) is calculated through Equation (4) [13]:

$$R_{SWI} = DOU/OPD \quad (4)$$

The ROL rate (nmol m^{-2} s^{-1}) from the roots of *V. spiralis* can be calculated using Equation (5):

$$\text{ROL rate} = \phi \times R_{SWI} \times L \times (L/2A + 1) \quad (5)$$

where L (mm) is half the width of the oxygenated zone and A (mm) is the average root diameter [13,47].

Images of the 2D O_2 distribution in the rhizosphere were drawn using Surfer software (Version 11.0, Golden Software, LLC, Golden, CO, USA). All O_2 concentration data in vertical O_2 profiles or 2D distribution images and ROL parameters are presented as "mean ± standard deviation (SD), n = 7". Statistical analyses were performed using SPSS software (Version 26.0, IBM Corporation, Armonk, NY, USA). The normality of data distributions was examined via the one-sample Kolmogorov–Smirnov test, and homogeneity of variance was assessed using Levene's test. All oxygen concentrations and ROL datasets conformed to a normal distribution and homoscedasticity ($p > 0.05$). One-way analysis of variance (one-way ANOVA) was used for comparisons among multiple data groups, with the significance level set at $p < 0.05$. Seven vertical oxygen profiles (Figure S2) for data analysis were selected from each image (Figure 2) at an interval of 0.70 cm. Each vertical profile contained 1300 data points.

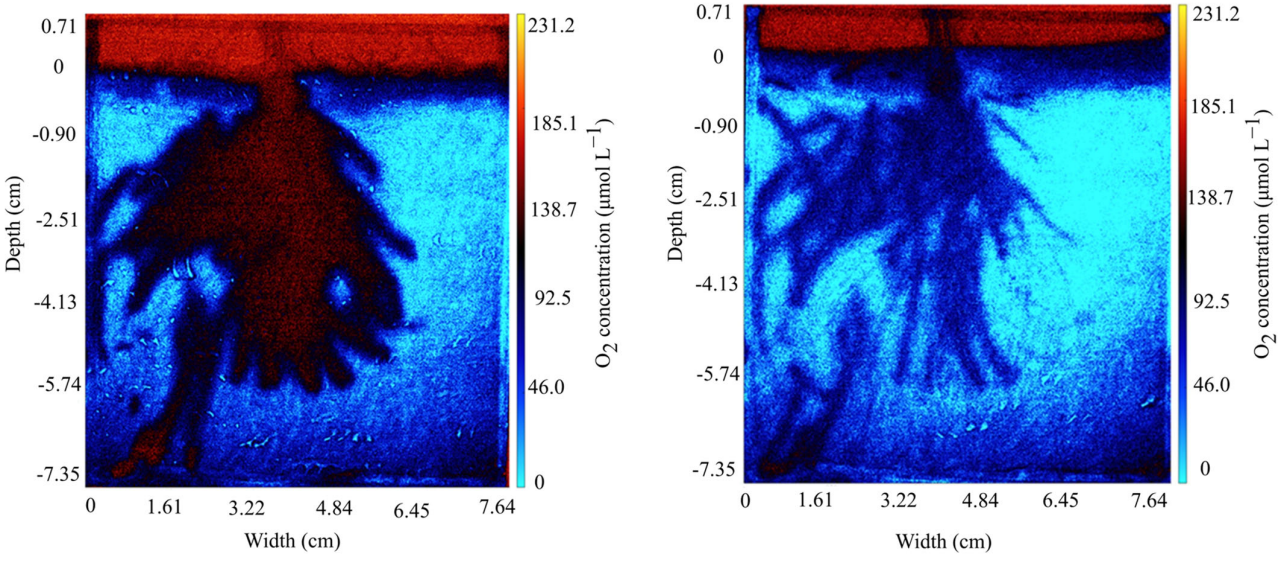


Figure 2. *Cont.*

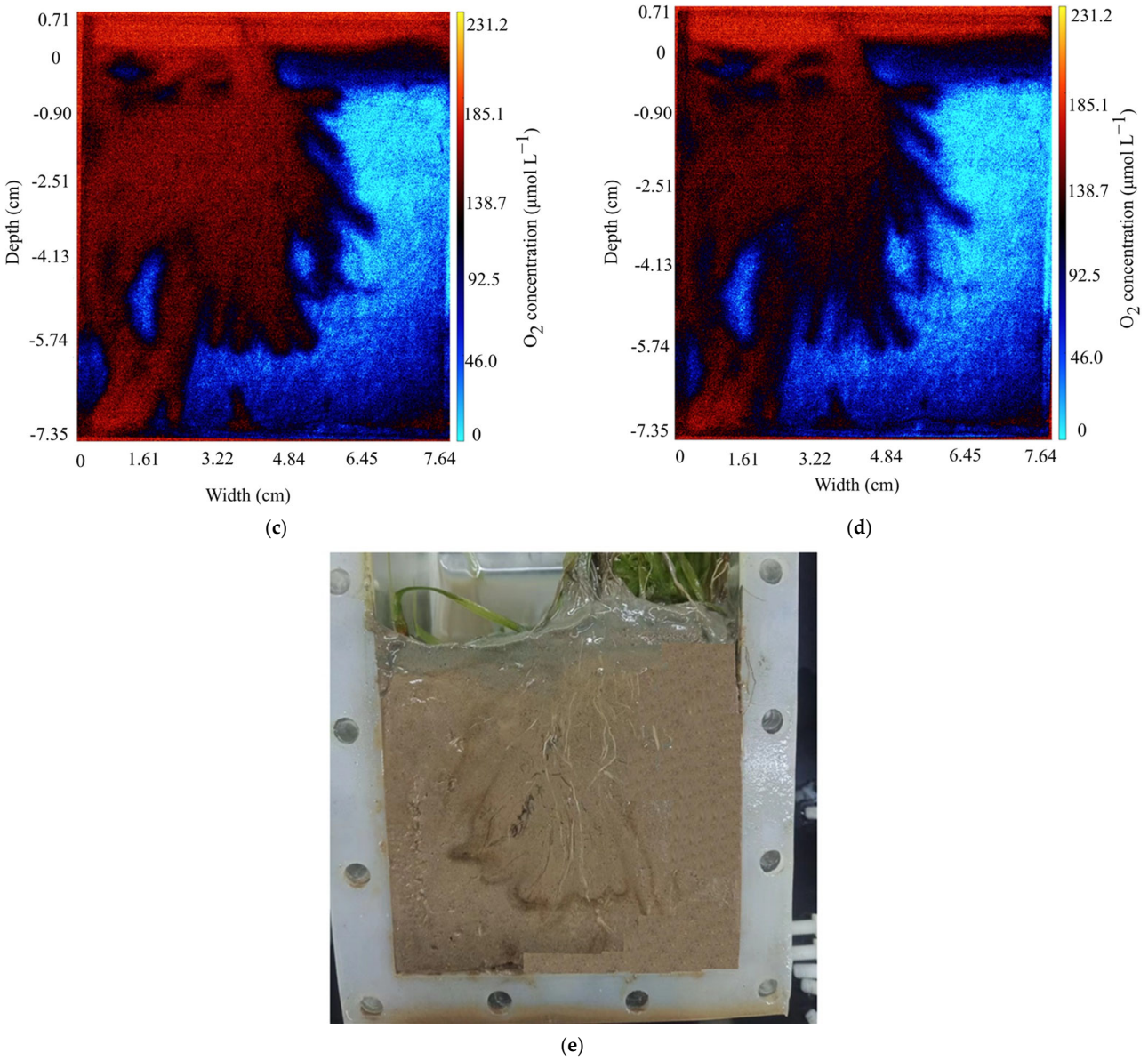


Figure 2. Images of the 2D distribution of O_2 in rhizosphere sediment under four environmental conditions of (**a**): high illumination/low O_2; (**b**): darkness/low O_2; (**c**): high illumination/high O_2 and (**d**): darkness/high O_2. (**e**): An image of roots and rhizosphere sediment. Notice: The "blue" and "red" colors in the color bars and subfigures (**a**–**d**) reflect the change in O_2 concentration from low to high levels.

3. Results

3.1. The Parameters for O_2 Dynamics in Rhizosphere Sediment

The O_2 concentration distributions in rhizosphere sediment under four environmental conditions are demonstrated in Figure 2. Differences in O_2 concentrations among (1) datasets in seven vertical profiles (Figure S2) in each sub-image (Figure 2) or (2) those in four subfigures (Figure 2) under the four environmental conditions were all statistically significant, as evaluated by one-way ANOVA ($p < 0.05$). The parameters for O_2 leakage in the rhizosphere are presented as "mean ± SD (n = 7)", as demonstrated in Table 1. OPD and DOU just below the SWI varied by 1.30 ± 0.20–11.14 ± 2.24 mm (n = 7) and 10.8 ± 1.6–14.3 ± 3.0 nmol m^{-2} s^{-1} (n = 7) under the four environmental conditions, respectively. R_{SWI} in the sediment ranged from 1.2 ± 0.2 to 1.8 ± 0.4 μmol m^{-3} s^{-1} (n = 7). ROL rates for three root parts under various environmental conditions followed the se-

quence: basal root > lateral root > root tip. Regarding environmental conditions, the ROL rate followed the sequence: high illumination/high O_2 > darkness/high O_2 > high illumination/low O_2 > darkness/low O_2 (Table 1).

Table 1. The average values of the width of the oxygenated zone at different surface positions (L), root diameter (A), O_2 penetration depth (OPD), diffusive O_2 uptake (DOU), volume-specific O_2 consumption (R_{SWI}) and radial O_2 loss rate (ROL rate). Note: The values are reported as mean ± SD (n = 7).

Environmental Condition	Rhizobox	OPD (mm)	DOU (nmol m^{-2} s^{-1})	R_{SWI} (μmol m^{-3} s^{-1})	ROL Rate (nmol m^{-2} s^{-1})	A (mm)	L (mm)
High illumination/low O_2	SWI	8.04 ± 0.98	14.3 ± 3.0	1.8 ± 0.4			
	Basal root	2.16 ± 0.32	–	–	32.2 ± 8.3	0.24 ± 0.02	3.02 ± 0.16
	Lateral root	1.94 ± 0.21	–	–	29.3 ± 7.3	0.20 ± 0.01	2.64 ± 0.14
	Root tip	1.76 ± 0.32	–	–	22.0 ± 6.2	0.16 ± 0.01	2.04 ± 0.12
Darkness/low O_2	SWI	6.45 ± 0.89	10.8 ± 1.6	1.7 ± 0.5			
	Basal root	1.85 ± 0.29	–	–	20.6 ± 5.1	0.24 ± 0.02	2.45 ± 0.14
	Lateral root	1.65 ± 0.25	–	–	14.1 ± 4.1	0.20 ± 0.01	1.83 ± 0.11
	Root tip	1.30 ± 0.20	–	–	13.1 ± 4.6	0.16 ± 0.01	1.59 ± 0.14
High illumination/high O_2	SWI	11.14 ± 2.24	13.8 ± 2.0	1.2 ± 0.2			
	Basal root	2.83 ± 0.38	–	–	49.6 ± 9.5	0.24 ± 0.02	4.71 ± 0.16
	Lateral root	2.22 ± 0.36	–	–	36.6 ± 8.3	0.20 ± 0.01	3.68 ± 0.19
	Root tip	1.94 ± 0.27	–	–	28.8 ± 6.4	0.16 ± 0.01	2.92 ± 0.16
Darkness/high O_2	SWI	8.95 ± 1.84	11.9 ± 1.6	1.3 ± 0.3			
	Basal root	2.31 ± 0.60	–	–	39.2 ± 7.5	0.24 ± 0.02	3.99 ± 0.15
	Lateral root	1.98 ± 0.28	–	–	36.2 ± 6.5	0.20 ± 0.01	3.51 ± 0.14
	Root tip	1.51 ± 0.22	–	–	22.7 ± 6.2	0.16 ± 0.01	2.58 ± 0.14

The vertical O_2 profiles derived from 2D images of the O_2 distribution in rhizosphere sediment and overlying water under the four environmental conditions are demonstrated in Figure 3. The sequence of the average O_2 concentration in rhizosphere sediment under the four environmental conditions was: high illumination/high O_2 (101.7 ± 2.3 μmol L^{-1}, n = 7) > darkness/high O_2 (88.2 ± 1.6 μmol L^{-1}, n = 7) > high illumination/low O_2 (79.8 ± 1.2 μmol L^{-1}, n = 7) > darkness/low O_2 (62.5 ± 1.2 μmol L^{-1}, n = 7). There were a lot of roots located at the surface rhizosphere sediment layer (depth: 0–−5 cm) (Figure 2e). The average O_2 (57.2 ± 1.0 μmol L^{-1}, n = 7) in surface rhizosphere sediment under darkness/low O_2 was significantly lower than 81.4 ± 1.2–104.1 ± 1.9 μmol L^{-1} (n = 7) under the other three conditions with high illumination and (or) O_2 in water (Figure 3) ($p < 0.05$). ROL rates (28.8 ± 6.4–49.6 ± 9.5 nmol m^{-2} s^{-1}, n = 7) under high illumination/high O_2 (Table 1) were significantly higher than 13.1 ± 4.6–39.2 ± 7.5 nmol m^{-2} s^{-1} (n = 7) under the other three conditions ($p < 0.05$). Furthermore, ROL rates under high illumination/high O_2 also corresponded to the largest O_2 peaks (111.4 ± 2.4 μmol L^{-1} at −3.196 cm, 103.7 ± 2.8 μmol L^{-1} at −4.523 cm, 101.6 ± 2.2 μmol L^{-1} at −5.354 cm, 117.6 ± 3.2 μmol L^{-1} at −7.052 cm, n = 7) in the vertical O_2 profile (Figure 3) of the four environmental conditions.

3.2. O_2 Dynamics in Rhizosphere Sediment and Around Different Root Parts

The oxygenated area (cm^2) for O_2 > 71 μmol L^{-1} (condition α) or >138 μmol L^{-1} (condition β) and the percent of the oxygenated area in the whole rhizosphere sediment (area %) under various environmental conditions were derived using Image. J. 1.53 software, as demonstrated in Figure 4. The largest area % values of 75.9% ± 3.2% (n = 7) for condition α and 25.7% ± 1.4% (n = 7) for condition β under high illumination/high O_2 of the four environmental conditions (Figure 4) corresponded to the highest ROL rate (28.8 ± 6.4–49.6 ± 9.5 nmol m^{-2} s^{-1}) (Table 1) and the average O_2 concentration (101.7 ± 2.3 μmol L^{-1}) in the rhizosphere sediment (Figure 3).

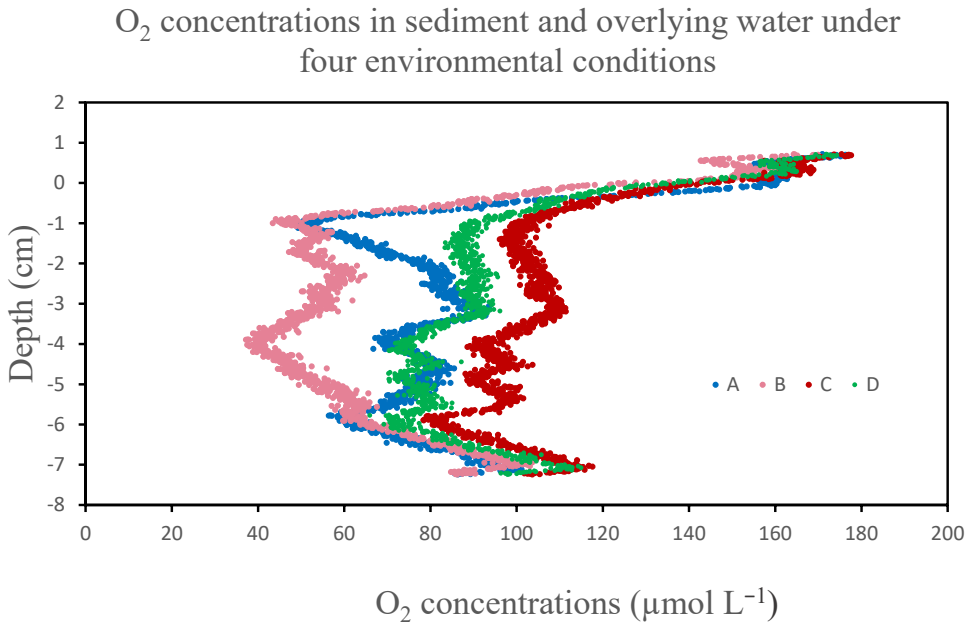


Figure 3. The vertical O_2 concentration profiles derived from 2D images of the O_2 distribution under four environmental conditions. A: high illumination/low O_2; B: darkness/low O_2; C: high illumination/high O_2 and D: darkness/high O_2.

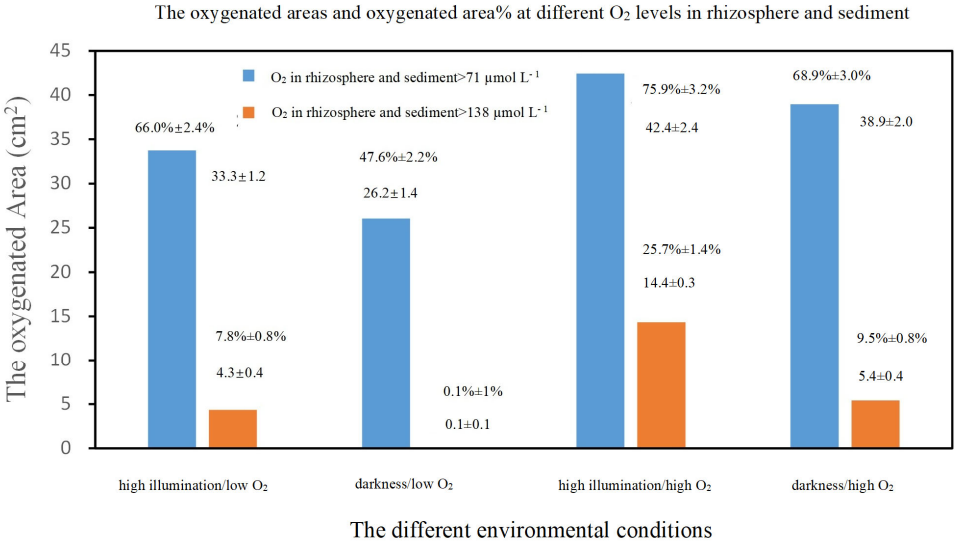


Figure 4. The oxygenated area (cm^2) for O_2 > 71 μmol L^{-1} (condition α) or >138 μmol L^{-1} (condition β) and the percent of those areas in the whole rhizosphere sediment zone (oxygenated area %) under four environmental conditions of high illumination/low O_2, darkness/low O_2, high illumination/high O_2 and darkness/high O_2.

The maximum O_2 concentrations for the lines transecting the basal root (1), root tip (2, 3, 4 or X) and lateral root (5, 6, 7 or 8) under the four conditions are demonstrated in Table 2. Images of the rhizosphere sediment, the locations of different roots and the related maximum O_2 concentrations in PO images under the four environmental conditions are demonstrated in Figure 5. The basal root (1) is the central root of *V. spiralis*, and it spreads downward in sediment (Figure 5a); the root tip (2, 3, 4 or X) on the right of Figure 5a is defined as a root segment with a distance of 0–1.5 mm from the root spire; the lateral root (5, 6, 7 or 8) on the left of Figure 5a is a branch root growing out of a base root. The distinct O_2 leakage from the root tip (X) can only be found in Figure 5d (high illumination/high O_2) and Figure 5e (darkness/high O_2).

Table 2. The maximum O_2 concentration on the line transecting the basal root, lateral root or root tip under high illumination/low O_2, darkness/low O_2, high illumination/high O_2 or darkness/high O_2 and the average O_2 concentration. Note: The average [1] is the averaged O_2 concentration for the basal root, lateral root or root tip for all four environmental conditions; the average [2] is the averaged O_2 concentration for the basal root, lateral root or root tip under each environmental condition. Note: The values are reported as mean ± SD (n = 7).

Root Classification	The Maximum O_2 Concentration in Each Root Line				The Average [1]
	High Illumination/Low O_2	Darkness/Low O_2	High Illumination/High O_2	Darkness/High O_2	(μmol L^{-1})
	(μmol L^{-1})	(μmol L^{-1})	(μmol L^{-1})	(μmol L^{-1})	
Base root					
1	160.0 ± 2.4	146.9 ± 1.9	172.1 ± 3.4	172.1 ± 4.6	162.8 ± 3.2
Root tip					
2	121.0 ± 1.9	97.4 ± 1.4	124.9 ± 2.2	111.4 ± 1.2	
3	121.2 ± 2.3	63.4 ± 1.1	114.9 ± 1.6	100.6 ± 1.2	
4	142.1 ± 2.2	107.4 ± 1.5	143.2 ± 2.8	114.8 ± 2.4	
X			141.4 ± 2.3	139.9 ± 2.4	
The average [2] (μmol L^{-1})	128.1 ± 2.3	89.4 ± 1.2	131.1 ± 2.9	116.7 ± 2.2	120.3 ± 2.3
Lateral root					
5	146.9 ± 3.0	101.7 ± 0.9	146.9 ± 3.2	121.6 ± 2.4	
6	171.8 ± 3.2	121.7 ± 2.4	171.8 ± 3.4	146.9 ± 3.2	
7	127.0 ± 2.3	100.8 ± 2.2	130.2 ± 2.8	125.5 ± 2.4	
8	119.1 ± 2.2	94.7 ± 1.6	165.4 ± 3.0	150.4 ± 3.2	
The average [2] (μmol L^{-1})	141.2 ± 3.4	104.7 ± 2.0	153.6 ± 3.2	136.1 ± 2.8	133.9 ± 2.4

For the basal root (1), the maximum O_2 concentration of 172.1 ± 2.4 μmol L^{-1} (n = 7) (root line 1) under high illumination/high O_2 or darkness/high O_2 was larger than 160.0 ± 2.2 μmol L^{-1} (n = 7) under high illumination/low O_2 and 146.9 ± 2.8 μmol L^{-1} (n = 7) under darkness/low O_2. In sum, the average O_2 maximum value for different root types under the four conditions (Table 2) followed the sequence: basal root > lateral root > root tip. The O_2 maximum in the basal root under the four conditions (Table 2) followed the sequence: high illumination/high O_2 = darkness/high O_2 > high illumination/low O_2 > darkness/low O_2. For the root tip and the lateral root, the average O_2 maximum under the four conditions (Table 2) followed the sequence: high illumination/high O_2 > high illumination/low O_2 > darkness/high O_2 > darkness/low O_2.

Four radial O_2 lines (a–d) transect across the different locations of a typical root surface, and line (e) is the longitudinal O_2 profile along this root axis, as demonstrated in Figure 6A. This root is extracted from root 5 under high illumination/low O_2 in Figure 5b. For the four lines (a–d) across the root, the maximum O_2 concentrations of 131.2 ± 2.4 μmol L^{-1} (n = 7) (line a), 141.2 ± 2.8 μmol L^{-1} (n = 7) (line b), 136.8 ± 3.2 μmol L^{-1} (n = 7) (line c) and 147.4 ± 3.7 μmol L^{-1} (n = 7) (line d) appeared in the root center; after that, they gradually dropped to the lowest values of 47.2 ± 1.4 μmol L^{-1} (line a), 50.3 ± 1.6 μmol L^{-1} (line b), 63.0 ± 2.0 μmol L^{-1} (line c) and 75.9 ± 2.2 μmol L^{-1} (line d) (n = 7) at the rhizosphere fringe (Figure 6B). The O_2 concentration distribution of the longitudinal O_2 profile (e) along the root axis with a length of 1.62 cm is demonstrated in Figure 6C. O_2 concentrations gradually decreased from a maximum of 160.9 ± 3.2 μmol L^{-1} (n = 7) at the top of the root axis to a minimum of 85.3 ± 2.4 μmol L^{-1} (n = 7) near the root tip. Altogether, (1) the sequence of the average O_2 concentrations in the basal root, lateral root and root tip under the four environmental conditions and (2) the sequence of O_2 concentrations in different locations on lines (a–e) in one typical root under high illumination/low O_2 are demonstrated in Table 3.

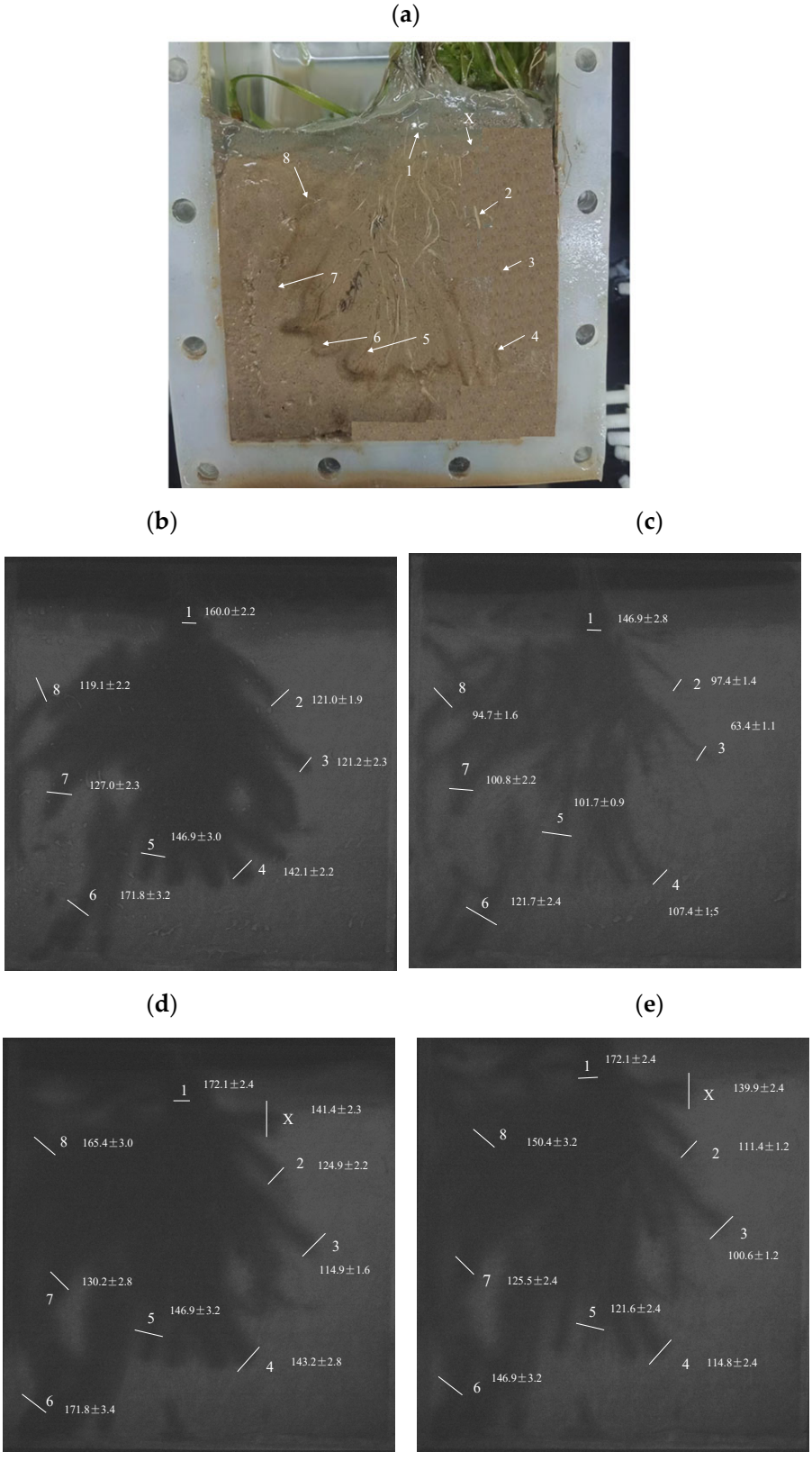


Figure 5. (**a**): The locations of nine roots in the root system of *V. spiralis* in a photograph. The locations of the line transecting the root tip, lateral root and basal root and the related maximum O_2 concentrations in 2D fluorescent images under four environmental conditions, including: (**b**): high illumination/low O_2, (**c**): darkness/low O_2, (**d**): high illumination/high O_2 and (**e**): darkness/high O_2.

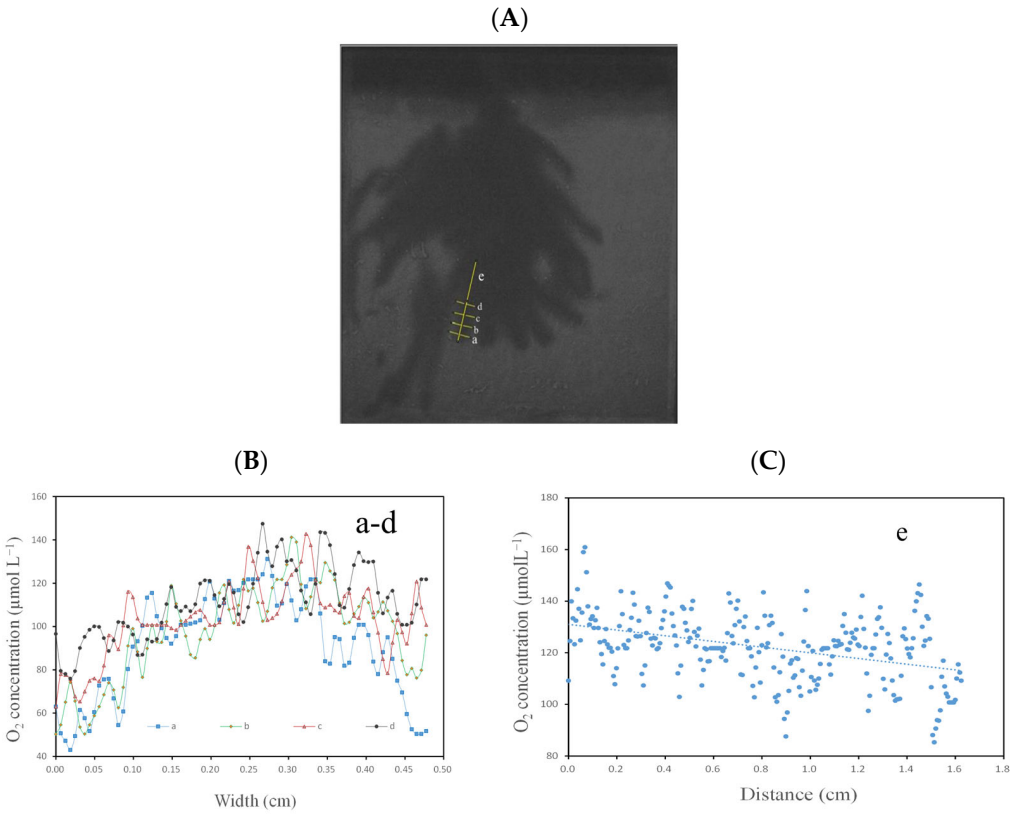


Figure 6. The cross-sectional profiles (a–d) for O_2 distribution across one typical root and the longitudinal line (e) for O_2 distribution along the root axis under high illumination/low O_2. (**A**): A fluorescent image of O_2 with one root and five lines (a–e); (**B**): O_2 distribution across the cross-sectional profiles (a–d) across the root; (**C**): O_2 distribution for the longitudinal line (e) along the root axis.

Table 3. The sequence of the average O_2 concentrations in the basal root, lateral root and root tip under four environmental conditions and the sequence of O_2 concentrations at different locations on lines (a–e) in one typical root under high illumination/low O_2. Note: The values are reported as mean ± SD (n = 7). Notice: The arrows and equals signs are used for numerical magnitude comparison.

Root Parts	The Average O_2 Concentration (μmol L^{-1})							
	All Four Conditions	**High Illumination/ High O_2**		**Darkness/High O_2**		**High Illumination/Low O_2**		**Darkness/Low O_2**
Basal root	162.8 ± 3.2 ↓	172.1 ± 3.4 ↓	=	172.1 ± 4.6 ↓	←	160.0 ± 2.4 ↓	←	146.9 ± 1.9 ↓
Lateral root	133.9 ± 2.4 ↓	153.6 ± 3.2 ↓	←	136.1 ± 2.8 ↓	→	141.2 ± 3.4 ↓	←	104.7 ± 2.0 ↓
Root tip	120.3 ± 2.3	131.1 ± 2.9	←	116.7 ± 2.2	→	128.1 ± 2.3	←	89.4 ± 1.2
Radial O_2 lines across root/O_2 concentration (μmol L^{-1})						Longitudinal O_2 profile/O_2 concentration (μmol L^{-1})		
Four lines (a–d)	root center			rhizosphere fringe		O_2 profile	top of root axis	near root tip
a	131.2 ± 2.4		→	47.2 ± 1.4		e	160.9 ± 3.2	→ 85.3 ± 2.4
b	141.2 ± 2.8		→	50.3 ± 1.6				
c	136.8 ± 3.2		→	63.0 ± 2.0				
d	147.4 ± 3.7		→	75.9 ± 2.2				

4. Discussion

4.1. O_2 Leakage Patterns and Oxidation Expansion in the Rhizosphere Characterized by ROL Parameters

O_2 leakage from *V. spiralis* led to conspicuous oxygenated zones around roots (Figure 2) [6,37]. O_2 concentrations were depleted significantly from the maximum in the root surface to the minimum in the rhizosphere fringe and bulk sediment (Figures 2 and 5),

and the reflected O_2 decrease was controlled by O_2 supply from leaf photosynthesis, O_2 in overlying water and transport through the porous root structure, and constant consumption in sediment [16,18,38]. The highest ROL rate and O_2 concentration (Figure 2; Tables 1 and 2) occurred locally around the basal root of the root system (basal root, lateral root and root tip). This was due to the shortest distance from the O_2 source to the basal root and the lowest O_2 consumption near the basal root [48] and its connection with O_2-enriched overlying water for downward O_2 diffusion [49,50]. The measured OPD range (1.30 ± 0.20–11.14 ± 2.24 mm) (Table 1) indicated that the thickness of the aerobic sediment layer increased along with the increment in illumination intensity or O_2 concentration in water. O_2 transport from leaf photosynthesis into overlying water and O_2 in overlying water from aeration can diffuse across the diffusive boundary layer and oxidize the upper layer of sediment, which leads to OPD in sediment [10], while O_2 transport from porous roots to rhizosphere sediment brings out OPD in the root system [13].

ROL capabilities differ significantly among different kinds of plants. The ROL rates of *V. spiralis* in this investigation (Table 1) are compared to other aquatic plants reported in some references [6,10,13,37,51]. The ROL rate values (13.1 ± 4.6–49.6 ± 9.5 nmol m^{-2} s^{-1}, n = 10) for *V. spiralis* in this experiment were comparable to 8.80 ± 7.32–30.34 ± 17.71 nmol m^{-2} s^{-1} in the other PO research on *V. spiralis* [6] and 28.90 ± 9.69–38.66 ± 18.03 nmol m^{-2} s^{-1} for another species (*Acorus calamus*) [10], lower than 5.32–122.69 nmol m^{-2} s^{-1} for rice roots [37] and 183.33–316.67 nmol m^{-2} s^{-1} for another species (*Littorella uniflora*) [51], and higher than 4.81 ± 1.73–13.05 ± 4.96 nmol m^{-2} s^{-1} for *Phragmites australis* [13], 17.24 ± 7.20–20.06 ± 8.58 for another species (*Oryza sativa*) [10] and 10.03 ± 3.64–13.03 ± 5.37 for *V. spiralis* [10]. The difference between *V. spiralis* and the plants reported in some references is due to interspecific differences in root morphology [52,53], different environmental conditions and PO images taken in different plant growth periods [6]. The well-developed aerenchyma and cortical porosity, and the large root diameter for plants such as rice [37] and *Acorus calamus* [10], improved diffusion and transport of O_2 towards the root. The various environmental conditions of light intensity [50] and O_2 aeration in overlying water [38] in the abovementioned plant cultivations can also lead to ROL diversity for those plants. According to the research results in references [6,51], ROLs of 30.34 ± 17.71 nmol m^{-2} s^{-1} for the young plants of *V. spiralis* [6] and 316.67 nmol m^{-2} s^{-1} for *Littorella uniflora* [51] were significantly higher than 8.80 ± 7.32 nmol m^{-2} s^{-1} and 183.33 nmol m^{-2} s^{-1} for their old roots, respectively. In this experiment, the high light intensity and O_2 concentration in overlying water favored O_2 leakage from the roots of *V. spiralis* [38]. ROL-derived O_2 release from *V. spiralis* roots diffused several mm into the sediment, which created an oxidized area around the roots (Figures 2 and 4; Table 1). The increased oxidized zone is important for the survival and quick growth of *V. spiralis* in anoxic and toxic sediments [38].

4.2. Influence of Irradiance and Oxygen in Overlying Water on O_2 Dynamics in the Rhizosphere

This investigation exactly detected and derived the ROL capabilities and O_2 distribution characteristics in the rhizosphere of *V. spiralis* by a high-resolution PO method. The 2D O_2 image, extracted 1D O_2 profile and ROL parameters have provided clear evidence for O_2 distribution variation along and across various root parts under four environmental conditions (Figures 2, 3 and 5; Tables 1 and 2). This result was consistent with that reported in references [10,13], which suggested that light intensity, O_2 level in overlying water and root morphology affected O_2 leakage dynamics in root systems, resulting in the characteristics of the oxygenated area and ROL parameters (OPD, DOU and ROL rate) of oxic roots in bulk anoxic sediment.

Root-induced O_2 leakage is the result of complex interactions between O_2 sinks and environmental conditions [22,25]. The lowest ROL rate, O_2 concentration in root parts

and oxygenated area % in rhizosphere sediment under darkness/low O_2 of the four environmental conditions (Figure 4; Tables 1 and 2) were attributed to (1) the lowest O_2 concentration in water for transfer to plant aerenchyma and (2) depletion in photosynthesis under darkness [6,10,13,49,52,53]. On the contrary, high illumination intensity enhanced the photosynthetic activity of *V. spiralis* leaves, and the high water O_2 level engendered the transfer of sufficient oxygen in the water column through the leaf and plant aerenchyma to the root, according to the research results in references [3,37,50,54–57]. So, the highest ROL rate, oxygenated area % in the rhizosphere and O_2 concentration in the root parts were observed under high illumination/high O_2 (Figure 5d; Tables 1 and 2). Though the values of oxygenated area % (Figure 4) related to the aerobic sphere in the rhizosphere under darkness/low O_2 and darkness/high O_2 were reduced, the aerobic sphere near the root parts was still maintained and did not disappear (Figure 5c,e). This suggested the adaptive ability of *V. spiralis* to deal with depleted photosynthetic activity, including (1) O_2 exchange between overlying water and aboveground plant parts (leaf and stem) in darkness [6,17] and (2) internal O_2 accumulation during photosynthesis to maintain root oxygenation in darkness [10,25].

ROL parameters (Table 1), O_2 concentrations in three root parts (Table 2), and oxygenated area % in the rhizosphere (Figure 4) under darkness/high O_2 were significantly higher than under darkness/low O_2. O_2 stored in roots and especially O_2 transfer from overlying water supplemented the O_2 level in the rhizosphere under darkness conditions, according to the research results in references [10,15]. Similar to *V. spiralis*, the roots of *Zostera marina* [18] and *Phragmites australis* [13] can also maintain O_2 leakage in the rhizosphere without photosynthesis when the overlying water remains aerobic.

4.3. Implications of the O_2 Gradient Across the Root Surface and the Longitudinal O_2 Distribution Along the Root Axis

The average O_2 maximum in the line transecting each kind of root followed the sequence basal root > lateral root > root tip under various environmental conditions (Table 3). This was due to the different distances from the O_2 source in the aboveground part of *V. spiralis* or overlying water to the different positions of the root parts mentioned above [16,48,57]. Exponential O_2 depletion from the root center (maximum O_2) to the fringe of the rhizosphere (minimum O_2) was found in each cross-sectional profile (a, b, c or d) across one typical root (Figure 6A,B). It was controlled by O_2 secreted from the root surface and enhanced O_2 consumption from the root surface to bulk sediment, for example, microbial respiration, chemical oxidation and organic decomposition [16,18,57]. A similar O_2 distribution gradient for a typical plant root has also been found in *Cymodocea rotundata* and *Zostera marina*, as reported in references [5,12].

O_2 was secreted from the root surface of *V. spiralis* and diffused into the rhizosphere sediment. This resulted in an aerobic area around lines (a–d) across the root axis (Figure 6A) with a width of 2.22 ± 0.10–3.20 ± 0.14 mm (n = 7) (Figure 6B). The average O_2 concentration for each radial line (a, b, c or d) continuously increased from 91.5 ± 5.9 μmol L^{-1} (n = 7) on line (a) at the root tip to 111.3 ± 6.2 μmol L^{-1} (n = 7) on line (d) at the top of the root (Figure 6B). The maximum O_2 (147.4 ± 3.7 μmol L^{-1}, n = 7) on line (d) at the top of the root decreased to 131.2 ± 2.4 μmol L^{-1} (n = 7) on line (a) at the root tip (Figure 6C and Table 3). Moreover, the O_2 concentration gradient on line (e) also demonstrated a depletion tendency from the top of the root to the root tip along the root axis (Figure 6C and Table 3). The distance from the aboveground part of *V. spiralis* to the root tip was longer than that of the top of this root, which caused the O_2 concentration at the top of the root to be larger than that at the root tip [16,57]. This has also been found for some plants, such as *Lobelia dortmanna* [58] and *Juncus effusus* [59], which exhibit significant O_2 release along the root axis. However, other plants, such as *Spartina anglica* [3] and *Potamogeton crispus* [17],

demonstrate the opposite ROL pattern, and their below-ground O_2 leakage is restricted to the root tip.

5. Conclusions

This research has visualized the complex dynamics of O_2 in the rhizosphere of *V. spiralis* in response to light/dark transitions and O_2 levels in overlying water using a high-resolution planar O_2 optode. The spatial heterogeneity in rhizosphere O_2 distribution and O_2 dynamics in different root parts under environmental fluctuations are revealed by 2D images of O_2 distribution, the derived 1D vertical O_2 profile and ROL parameters. The O_2 dynamics in the rhizosphere are highly changeable and depend on light irradiance and O_2 concentration in overlying water. The O_2 concentration distribution and ROL rate for different root parts and oxygenated area % in rhizosphere sediment decrease significantly, along with the depletion of illumination intensity or O_2 concentration in overlying water. Photosynthesis-derived O_2 production under illumination, the O_2 gradient between overlying water and sediment, and O_2 transfer to plant aerenchyma and roots influence O_2 distribution patterns in the rhizosphere, ROL rates and oxygenated area %. The O_2 level in water has a more distinct effect on the ROL of *V. spiralis* than the illumination–darkness transition. The ROL rate and O_2 concentration for three root parts follow the sequence basal root > lateral root > root tip, which is due to the different distances from the O_2 source in the aboveground part of *V. spiralis* or overlying water to the root part (basal root, lateral root or root tip). O_2 consumption in rhizosphere sediment and O_2 secretion from the root surface lead to a maximum O_2 concentration in the root center and a minimum in the rhizosphere fringe.

Altogether, O_2 leakage from roots to the rhizosphere is influenced by light–darkness and the exchange between water O_2 and plant tissues (leaf and stem). The various ROL characteristics and O_2 dynamics in different root parts and the rhizosphere reflect the resilience and ecological adaptability of *V. spiralis* in O_2-deficient sediment. The planar O_2 optode has been proven to be an excellent 2D visualization tool for highly dynamic ROL in heterogeneous oxidation-reduction rhizosphere sediment. Further research should be devoted to investigating the effects of temperature and altitude of water bodies on ROL, the uptake, transfer and transformation of nutrients in response to ROL in rhizosphere sediment, and the phytoremediation mechanism of macrophyte roots.

Supplementary Materials: The following supporting information can be downloaded at https://www.mdpi.com/article/10.3390/plants15131935/s1, Figure S1: The location of one sampling site at Qing River in Beijing (China). The map is derived by Google Earth Pro (Version 7.3.7); Figure S2: (A): The locations for seven O_2 vertical profiles in each image (Such as Figure 2a) for derivation of $\partial C/\partial Z$ and DOU or data analysis in Section 2.4 in text; (B): The locations for seven O_2 vertical profiles in rhizosphere sediment in each image (such as Figure 2a) for data analysis in Section 2.4 in text.

Author Contributions: Conceptualization, J.T., Z.W., W.J. and X.Y.; methodology, J.T., Z.W., W.J. and X.Y.; software, Z.W., X.Y. and Y.Z.; validation, Z.W., X.Y. and Q.C.; formal analysis, J.T., W.J. and Y.Z.; investigation, J.T., Z.W., W.J. and X.Y.; resources, W.J. and Q.C.; data curation, Z.W., W.J., Q.C. and X.Y.; writing—original draft preparation, J.T., Z.W. and W.J.; writing—review and editing, J.T., Z.W., W.J. and X.Y.; visualization, Y.Z. and X.Y.; supervision, J.T., W.J. and Q.C.; project administration, W.J. and Q.C.; funding acquisition, X.Y. and Z.W. All authors have read and agreed to the published version of the manuscript.

Funding: This research was funded by the National Key R&D Program of China (2022YFC3204004) and the National Natural Science Foundation of China (No. 42177219). The APC was funded by the National Key R&D Program of China (2022YFC3204004).

Data Availability Statement: The original contributions presented in this study are included in the article/Supplementary Materials. Further inquiries can be directed to the corresponding author.

Acknowledgments: The authors thank Qian Wang at EasySensor Ltd. (Nanjing, Jiangsu province, China) for suggestions on the PO measurement method.

Conflicts of Interest: The authors declare no conflicts of interest.

Abbreviations

The following abbreviations are used in this manuscript:

V. spiralis	*Vallisneria spiralis*
ROL	radial oxygen loss
2D	two-dimensional
PO	planar optode
TP	total phosphorus P
TN	total nitrogen
TFe	total iron
CMOS	complementary metal oxide semiconductor
LED	light-emitting diode
OPD	O_2 penetration depth
DOU	diffusive O_2 uptake
R_{SWI}	volume-specific O_2 consumption

References

1. Colmer, T.D. Long-distance transport of gases in plants: A perspective on internal aeration and radial oxygen loss from roots. *Plant Cell Environ.* **2003**, *26*, 17–36.
2. Ejiri, M.; Sawazaki, Y.; Shiono, K. Some Accessions of Amazonian Wild Rice (Oryza glumaepatula) Constitutively Form a Barrier to Radial Oxygen Loss along Adventitious Roots under Aerated Conditions. *Plants* **2020**, *9*, 880. [CrossRef] [PubMed]
3. Koop-Jakobsen, K.; Wenzhofer, F. The dynamics of plant-mediated sediment oxygenation in *Spartina anglica* rhizospheres—A planar optode study. *Estuaries Coasts* **2015**, *38*, 951–963.
4. Williams, P.N.; Santner, J.; Larsen, M.; Lehto, N.J.; Oburger, E.; Wenzel, W.; Glud, R.N.; Davison, W.; Zhang, H. Localized flux maxima of arsenic, lead, and iron around root apices in flooded lowland rice. *Environ. Sci. Technol.* **2014**, *48*, 8498–8506. [CrossRef] [PubMed]
5. Pedersen, O.; Borum, J.; Duarte, C.M.; Fortes, M.D. Oxygen dynamics in the rhizosphere of *Cymodocea rotundata*. *Mar. Ecol. Prog. Ser.* **1998**, *169*, 283–288. [CrossRef]
6. Han, C.; Ren, J.H.; Tang, H.; Xua, D.; Xie, X.C. Quantitative imaging of radial oxygen loss from *Valisneria spiralis* roots with a fluorescent planar optode. *Sci. Total Environ.* **2016**, *569*, 1232–1240. [CrossRef] [PubMed]
7. Brodersen, K.E.; Nielsen, D.A.; Ralph, P.J.; Kuhl, M. Oxic microshield and local pH enhancement protects *Zostera muelleri* from sediment derived hydrogen sulphide. *New Phytol.* **2015**, *205*, 1264–1276. [PubMed]
8. Jiménez, J.d.l.C.; Pellegrini, E.; Pedersen, O.; Nakazono, M. Radial Oxygen Loss from plant roots-methods. *Plants* **2021**, *10*, 2322–2336. [PubMed]
9. Morini, L.; Ferrari, C.; Bartoli, M.; Zilius, M.; Broman, E.; Visioli, G. *Vallisneria spiralis* L. adaptive capacity improves pore water chemistry and increases potential nitrification in organic polluted sediments. *Ecol. Process.* **2024**, *13*, 26–43. [CrossRef]
10. Zheng, Y.; Zhang, Z.H.; Sun, Y.; Wang, Z.D.; Chen, J.N.; Serdyanjiv, N.; Batdelger, O.; Han, C. High-resolution characterization of rhizosphere oxygen (O_2) dynamics in different wetland plant species after light/dark transitions. *Flora* **2025**, *323*, 152674–152683.
11. Connell, E.L.; Colmer, T.D.; Walker, D.I. Radial oxygen loss from intact roots of *Halophila ovalis* as a function of distance behind the root tip and shoot illumination. *Aquat. Bot.* **1999**, *63*, 219–228. [CrossRef]
12. Huang, W.; Yang, X.X.; Chen, H.J.; Lu, C.Y.; Che, F.F. Promoting effect of submerged plants on phosphorus source and sink in sediments: Response of phosphorus release and microbial community to Vallisneria natans and Potamogeton malaianus growth. *Environ. Technol. Innov.* **2024**, *36*, 103899. [CrossRef]
13. Li, C.; Ding, S.M.; Ma, X.; Chen, M.S.; Zhong, Z.L.; Zhang, Y.; Ren, M.Y.; Zhang, M.; Yang, L.Y.; Rong, N.; et al. O_2 distribution and dynamics in the rhizosphere of *Phragmites australis*, and implications for nutrient removal in sediments. *Environ. Pollut.* **2021**, *287*, 117193–117201. [CrossRef] [PubMed]

14. Caffrey, J.M.; Kemp, W.M. Seasonal and spatial patterns of oxygen production, respiration and root rhizome release in *Potamogeton-perfoliatus* L. and *Zostera-marina* L. *Aquat. Bot.* **1991**, *40*, 109–128. [CrossRef]
15. Han, C.; Ren, J.H.; Wang, Z.D.; Yang, S.K.; Ke, F.; Xu, D.; Xie, X.C. Characterization of phosphorus availability in response to radial oxygen losses in the rhizosphere of *Vallisneria spiralis*. *Chemosphere* **2018**, *208*, 740–748. [CrossRef] [PubMed]
16. Laskov, C.; Horn, O.; Hupfer, M. Environmental factors regulating the radial oxygen loss from roots of *Myriophyllum spicatum* and *Potamogeton crispus*. *Aquat. Bot.* **2006**, *84*, 333–340. [CrossRef]
17. Han, C.; Ren, J.H.; Williams, P.N.; Ke, F.; Shen, Q.S.; Wang, Z.D.; Xu, D.; Luo, J. High-resolution imaging of rhizosphere oxygen (O_2) dynamics in *Potamogeton crispus*: Effects of light, temperature and O_2 content in overlying water. *Plant Soil* **2019**, *441*, 613–627. [CrossRef]
18. Jensen, S.I.; Kuhl, M.; Glud, R.N.; Jorgensen, L.B.; Prieme, A. Oxic microzones and radial oxygen loss from roots of *Zostera marina*. *Mar. Ecol. Prog. Ser.* **2005**, *293*, 49–58. [CrossRef]
19. Tian, C.C.; Wang, C.B.; Tian, Y.Y.; Wu, X.Q.; Xiao, B.D. Root radial oxygen loss and the effects on rhizosphere microarea of two submerged plants. *Pol. J. Environ. Stud.* **2015**, *24*, 1795–1802. [CrossRef]
20. Satoh, H.; Okabe, S. Spatial and temporal oxygen dynamics inmacrofaunal burrows in sediments: A review of analytical tools and observational evidence. *Microbes Environ.* **2013**, *28*, 166–179. [PubMed]
21. Wang, X.D.; Wolfbeis, O.S. Optical methods for sensing and imaging oxygen: Materials, spectroscopies and applications. *Chem. Soc. Rev.* **2014**, *43*, 3666–3761. [CrossRef] [PubMed]
22. Li, C.; Ding, S.; Yang, L.; Zhu, Q.; Chen, M.; Tsang, D.C.W.; Cai, G.; Feng, C.; Wang, Y.; Zhang, C. Planar optode: A two-dimensional imaging technique for studying spatial-temporal dynamics of solutes in sediment and soil. *Earth-Sci. Rev.* **2019**, *197*, 102916–102934. [CrossRef]
23. He, Y.; Ding, N.; Yu, G.; Sunahara, G.I.; Lin, H.; Zhang, X.H.; Ullah, H.; Liu, J. High-resolution imaging of O_2 dynamics and metal solubilization in the rhizosphere of the hyperaccumulator *Leersia hexandra Swartz*. *J. Hazard. Mater.* **2023**, *455*, 131580–131589. [CrossRef]
24. Santner, J.; Larsen, M.; Kreuzeder, A.; Glud, R.N. Two decades of chemical imaging of solutes in sediments and soils-a review. *Anal. Chim. Acta* **2015**, *878*, 9–42. [CrossRef] [PubMed]
25. Ge, Z.; Ma, Z.; Hong, W.; Liu, K.; Yan, S.; Song, W.; Zhang, J. Temporal variations in reactive oxygen species in biofilms of submerged macrophytes: The key role of microbial metabolism mediated by oxygen fluctuations. *J. Hazard. Mater.* **2024**, *461*, 132542–132552. [CrossRef] [PubMed]
26. Nyer, S.C.; Volkenborn, N.; Aller, R.C.; Graffam, M.; Zhu, Q.; Price, R.E. Nitrogen transformations in constructed wetlands: A closer look at plant–soil interactions using chemical imaging. *Sci. Total Environ.* **2022**, *816*, 151560–151573. [CrossRef] [PubMed]
27. Huang, W.; Dong, X.S.; Tu, C.Q.; Yang, H.R.; Chang, Y.S.; Yang, X.X.; Chen, H.J.; Che, F.F. Response mechanism of sediment endogenous phosphorus release to functional microorganisms and its cyanobacterial growth and disappearance effects. *Sci. Total Environ.* **2024**, *906*, 167676. [PubMed]
28. Kuzyakov, Y.; Razavi, B.S. Rhizosphere size and shape: Temporal dynamics and spatial stationarity. *Soil Biol. Biochem.* **2019**, *135*, 343–360. [CrossRef]
29. Li, C.; Ding, S.M.; Chen, M.S.; Zhong, Z.L.; Sun, Q.; Wang, Y. Visualizing biogeochemical heterogeneity in soils and sediments: A review of advanced micro-scale sampling and imaging methods. *Crit. Rev. Environ. Sci. Technol.* **2023**, *53*, 1229–1253.
30. Staal, M.; Borisov, S.M.; Rickelt, L.F.; Klimant, I.; Kuhl, M. Ultrabright planar optodes for luminescence life-time based microscopic imaging of O_2 dynamics in biofilms. *J. Microbiol. Methods* **2011**, *85*, 67–74. [CrossRef] [PubMed]
31. Holst, G.; Kohls, O.; Klimant, I.; Konig, B.; Kuhl, M.; Richter, T. A modular luminescence lifetime imaging system for mapping oxygen distribution in biological samples. *Sens. Actuat. B-Chem.* **1998**, *51*, 163–170. [CrossRef]
32. Kűhl, M.; Holst, G.; Larkum, A.W.; Ralph, P.J. Imaging of oxygen dynamics within the endolithic algal community of the massive coral *Porites lobata*. *J. Phycol.* **2008**, *44*, 541–550. [PubMed]
33. Kűhl, M.; Rickelt, L.F.; Thar, R. Combined imaging of bacteria and oxygen in biofilms. *Appl. Environ. Microbiol.* **2007**, *73*, 6289–6295. [CrossRef] [PubMed]
34. Volkenborn, N.; Polerecky, L.; Wethey, D.S.; Woodin, S.A. Oscillatory porewater bioadvection in marine sediments induced by hydraulic activities of *Arenicola marina*. *Limnol. Oceanogr.* **2010**, *55*, 1231–1247. [CrossRef]
35. Koop-Jakobsen, K.; Mueller, P.; Meier, R.J.; Liebsch, G.; Jensen, K. Plant-Sediment interactions in Salt Marshes-an Optode Imaging study of O_2, pH, and CO_2 gradients in the rhizosphere. *Front. Plant Sci.* **2018**, *9*, 541–641. [CrossRef] [PubMed]
36. Li, C.; Ding, S.M.; Chen, M.S.; Sun, Q.; Zhang, Y.; Ma, X.; Zhong, Z.L.; Tsang, D.C.W.; Wang, Y. Mechanistic insights into trace metal mobilization at the micro-scale in the rhizosphere of *Vallisneria spiralis*. *Sci. Total Environ.* **2022**, *806*, 150735–150745. [CrossRef] [PubMed]
37. Chang, Y.S.; Wang, S.H.; Che, F.F.; Dong, X.S.; Yang, X.X.; Chen, H.J.; Huang, W. Arsenic Source-Sink Dynamics under Phosphorus Competition in Sediments from River-Lake Connected Systems. *Environ. Sci. Process. Impacts* **2025**, *27*, 706. [CrossRef] [PubMed]

38. Marzocchi, U.; Benelli, S.; Larsen, M.; Bartoli, M.; Glud, R.N. Spatial heterogeneity and short-term oxygen dynamics in the rhizosphere of *Vallisneria spiralis*: Implications for nutrient cycling. *Freshw. Biol.* **2019**, *64*, 532–543. [CrossRef]
39. Koop-Jakobsen, K.; Meier, R.J.; Mueller, P. Plant-Mediated rhizosphere oxygenation in the native invasive salt marsh grass *Elymus athericus*. *Front. Plant Sci.* **2021**, *12*, 669751–669760. [CrossRef] [PubMed]
40. Heilman, M.; Carlton, R.G. Methane oxidation associated with submerged vascular macrophytes and its impact on plant diffusive methane flux. *Biogeochemistry* **2001**, *52*, 207–224. [CrossRef]
41. Xing, X.; Ding, S.; Liu, L.; Chen, M.; Yan, W.; Zhao, L.; Zhang, C. Direct evidence for the enhanced acquisition of phosphorus in the rhizosphere of aquatic plants: A case study on Vallisneria natans. *Sci. Total Environ.* **2018**, *616–617*, 386–396. [CrossRef] [PubMed]
42. Borisov, S.M.; Klimant, I. Luminescent nanobeads for optical sensing and imaging of dissolved oxygen. *Microchim. Acta* **2009**, *164*, 7–15.
43. Zhu, Q.; Aller, R.C. A rapid response, planar fluorosensor for measuring two-dimensional pCO_2 distributions and dynamics in marine sediments. *Limnol. Oceanogr.-Methods* **2010**, *8*, 326–336. [CrossRef]
44. Glud, R.N. Oxygen dynamics of marine sediments. *Mar. Biol. Res.* **2008**, *4*, 243–289. [CrossRef]
45. Zhang, H.; Lombi, E.; Smolders, E.; Mcgrath, S. Kinetics of Zn release in soils and prediction of Zn concentration in plants using diffusive gradients in thin films. *Environ. Sci. Technol.* **2004**, *38*, 3608–3613. [CrossRef] [PubMed]
46. Ullman, W.J.; Aller, R.C. Diffusion coefficients in nearshore marine sediments. *Limnol. Oceanogr.* **1982**, *27*, 552–556. [CrossRef]
47. Fenchel, T. Worm burrows and oxic microniches in marine sediments. 1. Spatial and temporal scales. *Mar. Biol.* **1996**, *127*, 289–295. [CrossRef]
48. Blossfeld, S.; Gansert, D.; Thiele, B.; Kuhn, A.J.; Lösch, R. The dynamics of oxygen concentration, pH value, and organic acids in the rhizosphere of *Juncus* spp. *Soil Biol. Biochem.* **2011**, *43*, 1186–1197. [CrossRef]
49. Koren, K.; Brodersen, K.E.; Jakobsen, S.L.; Kuhl, M. Optical sensor nanoparticles in artificial sediments-a new tool to vsualize O_2 dynamics around the rhizome and roots of seagrasses. *Environ. Sci. Technol.* **2015**, *49*, 2286–2292. [CrossRef] [PubMed]
50. Jovanovic, Z.; Pedersen, M.O.; Larsen, M.; Kristensen, E.; Glud, R.N. Rhizosphere O_2 dynamics in young *Zostera marina* and *Ruppia maritima*. *Mar. Ecol. Prog. Ser.* **2015**, *518*, 95–105. [CrossRef]
51. Christensen, P.B.; Revsbech, N.P.; Sandjensen, K. Microsensor analysis of oxygen in the rhizosphere of the aquatic macrophyte Littorella uniflora ascherson. *Plant Physiol.* **1994**, *105*, 847–852. [CrossRef] [PubMed]
52. Colmer, T.D.; Pedersen, O. Oxygen dynamics in submerged rice (*Oryza sativa*). *New Phytol.* **2008**, *178*, 326–334. [CrossRef] [PubMed]
53. Wang, W.L.; Han, R.M.; Wan, Y.J.; Liu, B.; Tang, X.Y.; Liang, B. Spatio-temporal patterns in rhizosphere oxygen profiles in the emergent plant species *Acorus calamus*. *PLoS ONE* **2014**, *9*, 98457–98466. [CrossRef]
54. Barber, J. A mechanism for water splitting and oxygen production in photosynthesis. *Nat. Plants* **2017**, *3*, 17041–17050. [CrossRef] [PubMed]
55. Brix, H.; Sorrell, B.K.; Orr, P.T. Internal pressurization and convective gas-flow in some emergent fresh-water macrophytes. *Limnol. Oceanogr.* **1992**, *37*, 1420–1433. [CrossRef]
56. Pedersen, O.; Sauter, M.; Colmer, T.D.; Nakazono, M. Regulation of root adaptive anatomical and morphological traits during low soil oxygen. *New Phytol.* **2021**, *229*, 42–49. [PubMed]
57. Blossfeld, S. Light for the dark side of plant life:-Planar optodes visualizing rhizosphere processes. *Plant Soil* **2013**, *369*, 29–32.
58. Lenzewski, N.; Mueller, P.; Meier, R.J.; Liebsch, G.; Jensen, K.; Koop-Jakobsen, K. Dynamics of oxygen and carbon dioxide in rhizospheres of Lobelia dortmanna–a planar optode study of belowground gas exchange between plants and sediment. *New Phytol.* **2018**, *218*, 131–141. [CrossRef] [PubMed]
59. Blossfeld, S.; Gansert, D. A novel non-invasive optical method for quantitative visualization of pH dynamics in the rhizosphere of plants. *Plant Cell Environ.* **2007**, *30*, 176–186. [PubMed]

Disclaimer/Publisher's Note: The statements, opinions and data contained in all publications are solely those of the individual author(s) and contributor(s) and not of MDPI and/or the editor(s). MDPI and/or the editor(s) disclaim responsibility for any injury to people or property resulting from any ideas, methods, instructions or products referred to in the content.